Journal of Materials Chemistry A

Efficient Urea Synthesis via One-Step N−C−N Coupling: Strong Metal-Support Interaction-Driven Planar Cu Clusters on Two-Dimensional Mo2C MXene

Journal:	*Journal of Materials Chemistry A*
Manuscript ID	TA-ART-04-2024-002393.R1
Article Type:	Paper
Date Submitted by the Author:	20-May-2024
Complete List of Authors:	Zhang, yue; Harbin Normal University, Chemistry Lu, Linguo; University of Puerto Rico, Department of Chemistry Zhao, Tiantian; Harbin Normal University, Chemistry Zhao, Jing-Xiang; Harbin Normal University, Chemistry Cai, Qinghai; Harbin Normal University, chemistry and chemical engineering Chen, Zhongfang; University of Puerto Rico, Chemistry

Efficient Urea Synthesis *via* One-Step N−C−N Coupling: Strong Metal-Support Interaction-Driven Planar Cu Clusters on Two-Dimensional Mo_2C MXene

Yue Zhang,[1] Linguo Lu,[2] Tiantian Zhao,[1] Jingxiang Zhao,[1,] Qinghai Cai,[1] Zhongfang Chen[2,*]*

[1] College of Chemistry and Chemical Engineering, and Key Laboratory of Photonic and Electronic Bandgap Materials, Ministry of Education, Harbin Normal University, Harbin, 150025, China

[2] Department of Chemistry, University of Puerto Rico, Rio Piedras Campus, San Juan, Puerto Rico 00931, USA

[*] To whom correspondence should be addressed. Email: *zhaojingxiang@hrbnu.edu.cn (J. Z.).; zhongfang.chen1@upr.edu (Z.C.)*

Abstract: The electrocatalytic co-reduction of small carbonaceous and nitrogenous molecules recently emerged as a promising strategy to mitigate carbon emissions, facilitate wastewater denitrification, and sustain urea synthesis. However, the development of highly efficient electrocatalysts to accelerate C–N coupling and multiple protonation steps remains challenging. Herein, inspired by the "strong metal-support interaction" (SMSI) concept, we designed novel catalysts, comprised of size-selected Cu clusters anchored on the two-dimensional molybdenum carbide MXene (Cu_n/Mo_2C), for urea production via the co-reduction of nitrate (NO_3^-) and carbon dioxide (CO_2). Our density functional theory (DFT) computations revealed that these Cu clusters are strongly immobilized on the Mo_2C substrate by forming planar structures, leading to considerable active sites. Notably, these Cu_n/Mo_2C catalysts demonstrate enhanced activity for urea synthesis through a one–step N–C–N coupling mechanism. This process involves the insertion of CO^* into the NH_2^*–NH_2^* intermediate, facilitated by electrostatic attractions between their nitrogen atoms. In particular, among the catalysts tested, Cu_4/Mo_2C exhibits superior performance, achieving urea production with a limiting potential of –0.36 V. Furthermore, the competing side reactions, such as CO reduction or release, NH_3 production, hydrogen evolution, and surface oxidation, are significantly suppressed, ensuring its high selectivity for urea synthesis. This work not only introduces a novel method for urea electro-synthesis *via* SMSI between metal clusters and substrate, but also suggests a strategy for synthesizing other organonitrogen compounds.

1. Introduction

Urea is a cornerstone in agriculture, serving as an extremely important nitrogenous fertilizer with a high nitrogen content of 46%.[1, 2] In addition, urea is a critical chemical feedstock for manufacturing plastics, drugs, textiles, and energy carriers,[3, 4] reflecting its integral role in various industrial processes. With the ever-increasing human population and surging demand for chemical synthesis, global urea production is expected to reach 211.5 million metric tons by 2026.[5] Currently, the prevailing industrial approach for urea synthesis is the energy-intensive Bosch–Meiser process,[6] which operates under severe conditions and relies on ammonia (NH_3) obtained from the Haber-Bosch method.[7] This conventional route consumes about 2% of the world's energy, and contributes to 1% global CO_2 emission, thereby exacerbating the energy crisis and environmental degradation.[8, 9] Therefore, there is a pressing need to develop alternative urea synthesis methodologies that operate under milder conditions and utilize renewable energy sources, paving the way for a more sustainable and environmentally benign urea production.

In this context, electrocatalytic urea synthesis emerges as an attractive alternative to traditional methods. This approach, driven by renewable electricity, exploits C–N coupling of nitrogenous species (such as NO_3^-, NO_2^-, NO, and N_2) with carbon sources (CO_2 and CO) to circumvent the need for NH_3 production.[10-13] In particular, the electrocatalytic C–N coupling between NO_3^- and CO_2/CO represents a promising "one stone, three birds" strategy that simultaneously addresses the reduction of carbon footprint, valorization of waste, and sustainable urea production.[14-17] In addition, NO_3^- is an attractive nitrogen source due to its lower dissociation energy, which facilitates its activation in NH_3 and urea synthesis

pathways.[18] However, urea formation via electrocatalysis is a complex multistep process, which involves three crucial steps, including co-adsorption of diverse reactants, C–N coupling, and subsequent protonation of various reaction intermediates.[19-24] This complexity presents significant challenges, and it is urgently needed to design highly efficient electrocatalysts for urea synthesis.

Tremendous recent efforts have been made to search for advanced electrocatalysts for urea synthesis. Wei *et al.* fabricated single Cu atoms on CeO_2 substrate and achieved an ultra-high urea yield rate of 52.84 mmol h^{-1} $g_{cat.}^{-1}$ at −1.6 V versus a reversible hydrogen electrode.[14] Mao *et al.* designed a novel carbon-supported indium-doped bismuth nanoparticle that leverages In dopants as active sites while also enhancing Bi's activity, synergically boosting the C–N coupling between CO^* and NH_2^*.[25] Zhang's group prepared self-supported oxygen vacancy-rich ZnO porous nanosheets and core–shell Cu@Zn nanowires, which exhibit superior performance toward urea synthesis from CO_2 and NO_3^- feedstocks.[10, 26] Theoretically, Wan *et al.* found that Cu (111) surface can efficiently catalyze urea production through co-reduction of NO and CO, and proposed a two-step C–N coupling mechanism involving CO^* + N^* and $CONH^*$ + N^*;[27] Jiao and co-workers designed triple-atom catalysts to advance urea formation through one-step N–C–N coupling.[28]

While these pioneering contributions underscored the potential of electrocatalytic urea synthesis, the exact C–N coupling mechanism (whether one-step or two-step) and the identification of coupling precursors remain controversial. In particular, further improvement in the catalytic performance for urea electrosynthesis is a formidable challenge.

Recently, a principle, namely, strong metal−support interaction, emerged and showed its increasing importance in diverse chemical processes.[33-37] SMSI usually features significant charge transfer and substantial orbital hybridization at the metal–support interface. These interactions lead to the formation of new chemical bonds and significantly alter the geometry and the electronic properties of catalysts, thereby influencing their stability and catalytic performance in heterogeneous catalysis.

Drawing on the SMSI principle and the well-documented potential of Cu-based materials for urea synthesis,[29-32] we proposed a new class of active and stable catalysts for urea production, which can facilitate urea electrocatalysis via the co-reduction of NO_3^- and CO_2, leveraging the SMSI effects between the Cu clusters and the support structure to enhance catalytic efficiency and stability. In pursuing the Cu-based SMSI phenomenon, we selected two-dimensional molybdenum carbide (Mo_2C) MXene as the support, which has been recognized as superior catalyst support (such as for Fe, Mo, and Pt) and exhibits comparative advantage over traditional carbon supports, including enhanced stability and durability.[38-41] Especially, the utilization of 2D Mo_2C MXene as a substrate in electrocatalysis offers various benefits: it ensures high conductivity to boost the electrocatalytic kinetics, provides abundant surface-exposed unsaturated Mo atoms for the robust anchoring of catalyst nanoparticles, and preserves the neutral state of metal atoms to effectively optimize their catalytic performance.[42-48] Thus, the integration of Cu-based nanoparticles with the Mo_2C substrate holds great promise for facilitating the strong interfacial electronic interaction and developing highly stable and efficient electrocatalysts for the advanced urea electrosynthesis by the co-reduction of NO_3^- and CO_2.

Herein, through comprehensive density functional theory (DFT) computations, we explored the catalytic potential of several size-selected Cu clusters anchored on a Mo_2C monolayer (Cu_n/Mo_2C, n = 1 ~ 7) for urea electrosynthesis from NO_3^- and CO_2. These results revealed a pronounced preference for these Cu clusters to adopt planar configurations on the Mo_2C substrate, a phenomenon accompanied by significant charge transfer and obvious orbital hybridization. Interestingly, our DFT computations suggested that these Cu_n/Mo_2C catalysts facilitate urea synthesis *via* a "one-step" N–C–N coupling mechanism, whereby CO^* is inserted into the NH_2^*–NH_2^* intermediate. This mechanism is thermodynamically and kinetically more favorable than the "two-step" C–N coupling. Among these candidates, Cu_4/Mo_2C exhibits slightly higher catalytic activity for urea synthesis with a relatively lower limiting potential of –0.36 V. This enhanced activity is coupled with a significant suppression of competing side reactions, thereby guaranteeing its high selectivity for urea production. Our findings not only present a promising new class of electrocatalysts for urea synthesis from the abundant C– and N–based small molecules but also expand the scope of SMSI applications in electrocatalysis.

2. Computational models and methods

All spin–polarized DFT computations were carried out utilizing the Vienna ab initio Simulation Package (VASP).[49, 50] The projector augmented wave (PAW) potential was employed to describe ion-electron interactions,[51, 52] while the exchange–correlation interactions were determined by the Perdew–Burke–Ernzerhof (PBE)[53] functional within the generalized gradient approximation (GGA). The cutoff energy was set to 550 eV for the plane

wave expansion. A given system was fully relaxed until reaching the convergence threshold of 10^{-5} eV for energy and 0.03 eV/Å for atomic forces. To accurately describe van der Waals (vdW) forces, we incorporated the DFT+D3 method.[54] The energy barriers for C–N coupling reactions were determined using the climbing image nudged elastic band (CI-NEB) method,[55] providing insight into the kinetic feasibility of the catalytic processes.

The Mo_2C MXene was modeled by a periodic hexagonal (4 × 4) supercell containing 16 C and 32 Mo atoms, which served as the substrate for the size-selected Cu clusters. A vacuum region of 25 Å was adopted to avoid interaction between periodic images. The Brillouin zone was sampled by a (3 × 3 × 1) mesh of *k*-points for structural relaxation and a denser (15 × 15 × 1) mesh for calculating electronic properties. Ab initio molecular dynamic (AIMD) simulations were performed in the NVT ensemble using the Nosé-Hoover thermostat,[56] spanning a duration of 10 ps with a time step of 2.0 fs.

The Gibbs free energy change (ΔG) for each elementary step involved in urea electrosynthesis was determined using the computational hydrogen electrode (CHE) model.[57, 58] Based on this model, the value of ΔG can be obtained by the formula: $\Delta G = \Delta E + \Delta ZPE - T\Delta S + \Delta G_{pH} + eU$, where ΔE is the reaction energy of the reactants and products adsorbed on the catalyst, calculated directly by DFT; ΔZPE and ΔS are the changes in zero point energy and entropy at 298.15 K, which can be calculated by the vibration frequency. ΔG_{pH} is the free energy correction of pH, which can be calculated by: $\Delta G_{pH} = K_B T \times pH \times ln10$. Note that for simplicity, the pH value was set to zero; U is the applied potential. The catalytic activity of urea formation was evaluated by using the

limiting potential (U_L), which was further calculated according to the free energy changes of each basic step as follows: $U_L = -\max(\Delta G_1, \Delta G_2, \Delta G_3, \Delta G_4 \ldots\ldots, \Delta G_i)/e$.

3. Results and discussion

3.1. Identifying SMSI for Cu_n/Mo_2C.

The 2D Mo_2C MXene features a sandwich-like structure, with a C layer nestled between two Mo layers. Specifically, the C atoms form an edge-shared Mo_6C octahedral structure with the exposed Mo atoms, having a C–Mo length of 2.09 Å (Fig. S1a). This configuration well aligns with findings from prior experimental and theoretical studies.[59-61] On the other hand, isolated Cu_n clusters exhibit two kinds of configurations when n exceeds 4: planar and three-dimensional (3D) structures. After full structural relaxation, we found that planar clusters are more stable for n < 7 (Fig. S1b), which is fully consistent with previous reports.[62-64]

Based on the optimized 2D Mo_2C MXene and different Cu clusters, we then constructed Cu_n/Mo_2C materials by placing different Cu_n clusters on the 2D Mo_2C support. Note that both planar and three-dimensional Cu_n configurations were considered. After full geometric relaxations, we identified the most stable Cu_n/Mo_2C, as shown in Fig. 1a and Fig. S2. To evaluate the stability of the catalysts, we computed the average binding energy (E_{bind}) of each Cu atom by: $E_{bind} = (E_{Cu_n/Mo_2C} - nE_{Cu} - E_{Mo_2C})/n$, where E_{Cu_n/Mo_2C}, E_{Cu}, E_{Mo_2C} represent the total electronic energies of Cu_n/Mo_2C materials, isolated Cu atom, and pristine Mo_2C monolayer, respectively. As depicted in Fig. 1b, the computed E_{bind} values for the planar Cu_n cluster are in the range from –3.77 to –4.07 eV, which are more negative than those of 3D

ones (–2.87~–3.74 eV). This suggests a pronounced preference for planar adsorption patterns of these Cu clusters on the Mo_2C substrate, manifesting the strong interaction of these Cu clusters on Mo_2C support, or the SMSI phenomenon. Structurally, all Cu atoms in these planar Cu clusters are anchored at the hollow sites of three-membered Mo rings, each forming three Cu–Mo bonds with an average length of about 2.67 Å. Compared with the freestanding Cu clusters and the pristine Mo_2C monolayer, the Cu–Cu and Mo–C bonds are elongated to different degrees due to the strong interaction between each other, yet without compromising their structural integrity.

To elucidate the robust binding of these Cu clusters on the Mo_2C support, we took Cu_4/Mo_2C as an example to carefully analyze the projected density of state (PDOSs). As shown in Fig. 1c, there is a strong hybridization between the Cu-3d and the Mo-4d states in the energy region from –4.64 to –0.31 eV. Moreover, the computed charge density difference, as shown in Fig. 1d, indicates a significant charge accumulation between the interfacial Cu and Mo atoms. Consistently, about 0.18 electrons are transferred from each Cu atom to the Mo_2C substrate, inferring a valence state of about +0.18 for the Cu atoms. Interestingly, a lower oxidation state and positive charge on metal atoms can enhance their ability to adsorb reactants,[65] and thus hold great potential for improving their catalytic performance.

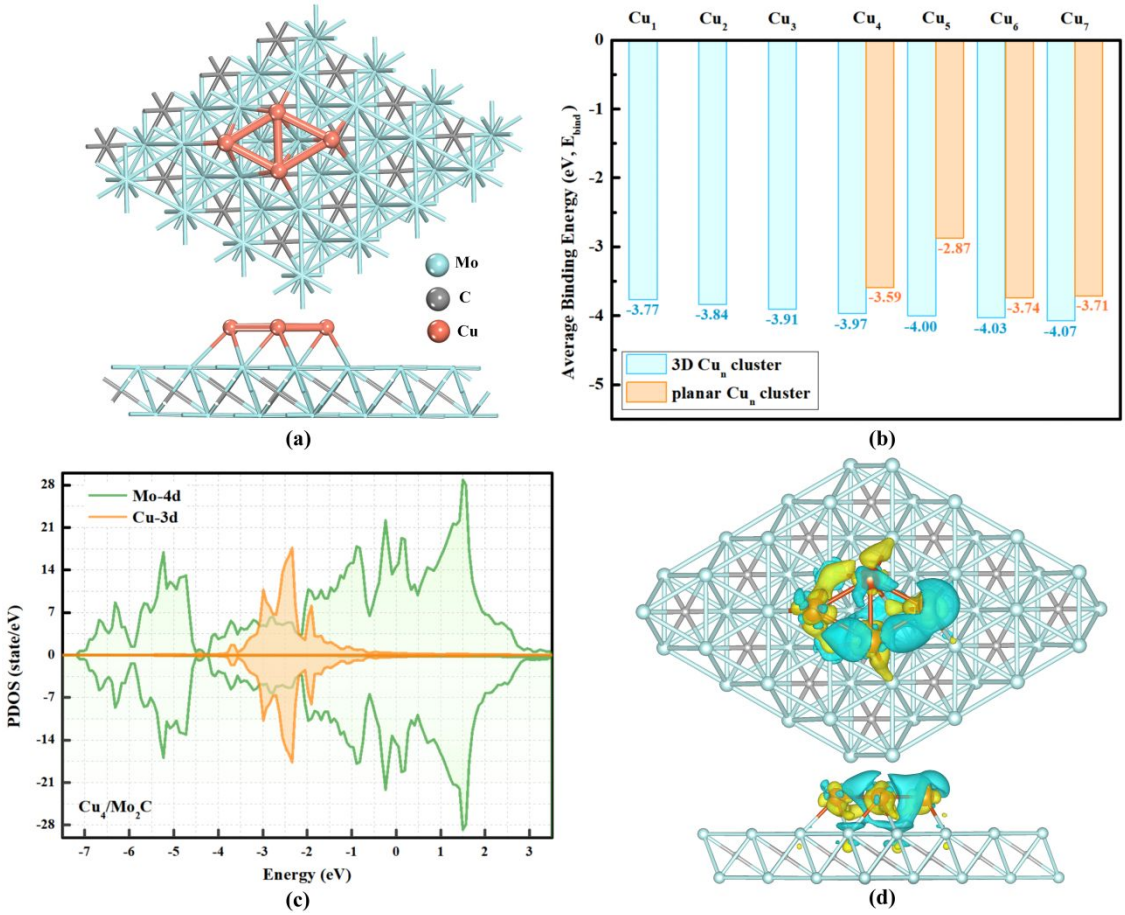

Fig. 1. (a) Top and side views of the optimized Cu_4/Mo_2C structure. (b) Computed average binding energy of Cu_n/Mo_2C materials, comparing the stability of planar and 3D configurations of Cu clusters. (c) Projected density of states (PDOSs) of the Cu_4/Mo_2C, detailing the hybridization between Cu-3d and Mo-4d orbitals. (d) Differential charge density plot of Cu_4/Mo_2C, with an isosurface value of 0.005 e $Å^{-3}$. Areas of electron accumulation are shown in yellow and regions of electron depletion in cyan.

3.2. Catalytic Activity of Cu_n/Mo_2C for Urea Formation.

Having established the SMSI of Cu_n clusters on Mo_2C and ensured their stability, we proceeded to explore their catalytic performance for urea synthesis.

Despite significant progress in this field, the underlying mechanism of C–N coupling—whether it proceeds via a one-step or a two-step process—remains a subject of debate. By joint experimental and theoretical studies, Wei *et al.* reported that urea formation occurs through a two-step C–N coupling pathway *via* $NO^* + CO^*$ and $ONCO^* + NO^*$ on the electrochemically reconstituted Cu_4 cluster active site anchored on a CeO_2 support.[14] By means of DFT computations, Wan *et al.* suggested two possible C–N coupling *via* $CO^* + N^*$ and $CONH^* + N^*$ for urea production on Cu(111) surface;[27] in contrast, Jiao and co-workers proposed a concurrent N–C–N coupling mechanism on the triplet-atom catalyst (supported on C_9N_4 monolayer), in which CO^* preferable inserts into NO^*-dimerization derived $NH_2^*–NH_2^*$ species.[28] Notably, the one-step mechanism may be materials-dependent. Obviously, there is no consensus on the predominant mechanism or the specific intermediates involved at present.

Our selection of Cu_4/Mo_2C as the model system was based on several crucial considerations. First, the Cu_4 cluster's square-like configuration, anchored on the Mo_2C, closely resembles the Cu(100) surface. This similarity is pivotal as the Cu(100) surface is known for its high catalytic activity in the C–N coupling during the electrocatalytic reduction of CO_2 and NO_3^-/NO_2^- towards urea formation,[66,67] facilitated by the Cu–Cu bridge site that can prompt C–N coupling between C– and N–based active reaction intermediates. Furthermore, as mentioned earlier, the choice of Mo_2C as a support is due to its exceptional stability and conductivity offered by its 2D structure, which is conducive to reinforce the metal-support interaction effect. Interestingly, the synergy between the planar Cu_4 cluster and 2D nanosheets has been validated by prior work to significantly enhance electrocatalytic efficiency. For example, Fan *et al.* reported that their fabricated planar Cu_4 cluster on the

template of Ti_9-oxo nanoring achieved notable selectivity in reducing CO_2 to C_2H_4 electrocatalytically.[68]

To this end, we utilized Cu_4/Mo_2C as a representative and examined both one-step and two-step mechanisms to ascertain the preferred C–N coupling pathway for urea synthesis. Noteworthy, previous experiments[69-71] have identified NO and CO as N– and C–containing adsorbates, respectively, which are key intermediates derived from the electrochemical reduction of NO_3^- and CO_2. Thus, the co-reduction of NO + CO was used as a model to investigate the C−N electrocatalytic coupling reactions, which is critical to developing advanced catalysts for the electrosynthesis of value-added organonitrogen compounds.

3.2.1. One-step mechanism

In the one-step mechanism, the co-adsorption of two NO and one CO molecules is a prerequisite for N–C–N coupling. Thus, we examined the adsorption of two NO and one CO molecules on the anchored Cu_4 cluster. As shown in Fig. 2a, we found that the (2NO + CO) can be separately chemisorbed on the planar Cu_4 cluster with a rather negative free energy change of –2.05 eV, forming the (NO^* + NO^* + CO^*) intermediate, where * represents the active site. However, the direction insertion of CO^* into the two adsorbed NO^* to form NO^*–CO–NO^* intermediate is endergonic by 0.63 eV (Fig. 2b), indicating that this N–C–N coupling is thermodynamically unfavorable. In contrast, the coupling of two adsorbed NO^* species to form NO^* dimerization (Fig. 2c) is thermodynamically feasible with a slightly negative ΔG value of –0.01 eV. Kinetically, the transformation of separated adsorbates (NO^* + NO^* + CO^*) into associated NO^*–NO^* complex with adjacent CO^* (NO^*–NO^* + CO^*) features a rather low

energy barrier of 0.18 eV (Fig. 2d). Thus, the formation of the (NO^*–NO^* + CO^*) intermediate is preferred both thermodynamically and kinetically.

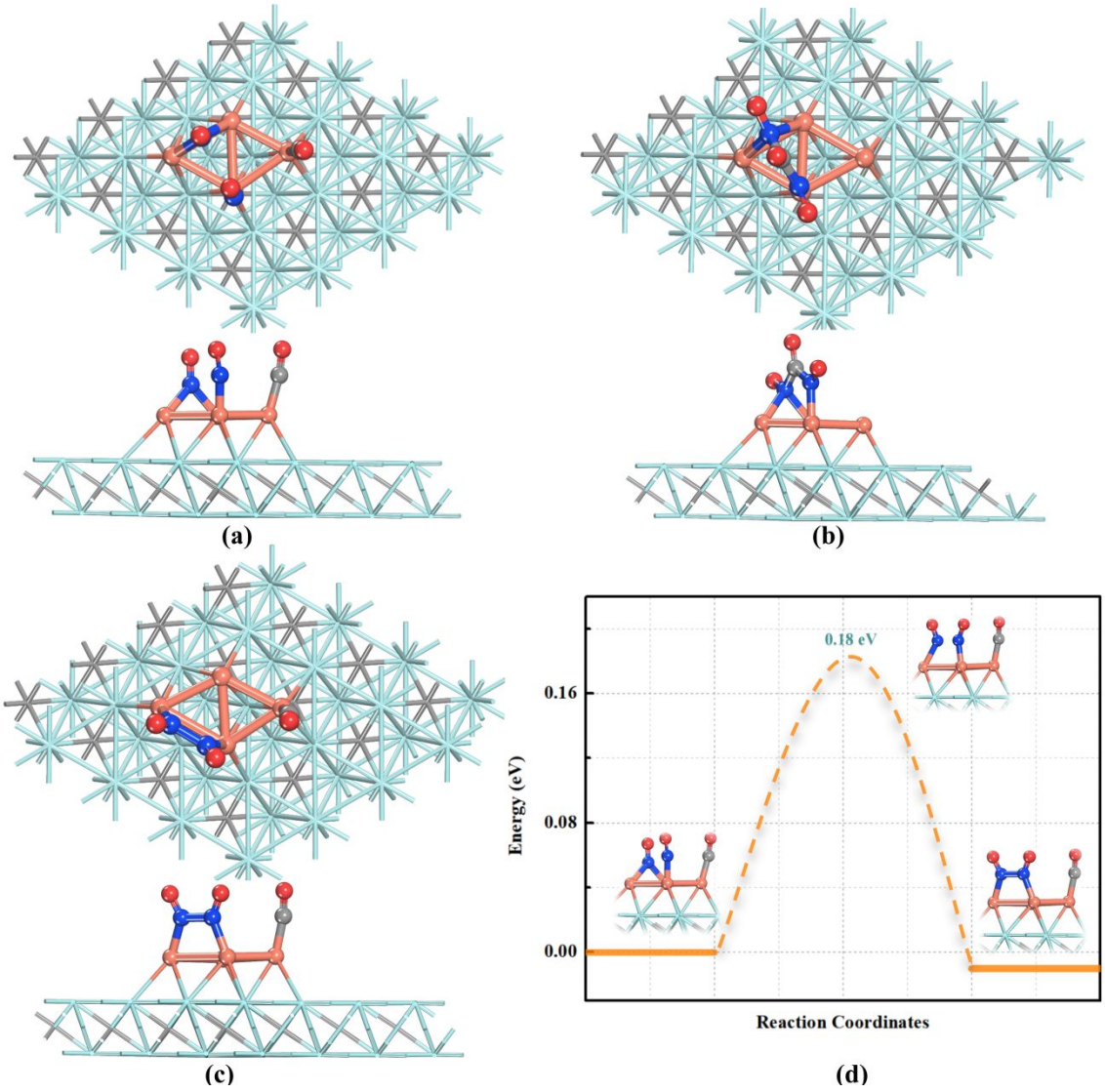

Fig. 2. Optimized structures for (a) NO^* + NO^*+ CO^*, (b) NO^*–CO^*–NO^*, and (c) NO^*–NO^*+CO^*. (d) The minimum energy pathway from (NO^* + NO^*+ CO^*) to (NO^*–NO^* + CO^*) and the corresponding energy barrier.

Following the formation of (NO^*–NO^* + CO^*) intermediate, we studied its subsequent transformation into urea *via* eight proton-coupled electron transfer (PCET) steps. The calculated free energy changes (ΔG) of all possible elementary steps are summarized in Table S1. In the following sections, we will focus on the energetically most favorable reaction pathway (Fig. 3), which exhibits the lowest positive free energy change between any two elementary steps. Thus, along this pathway, the required applied voltage is the least negative to make the whole reaction exergonic, thereby establishing the limiting potential.

Starting from the formed (NO^*–NO^* + CO^*) complex, the first three hydrogenation steps are all exergonic. The first hydrogen step readily occurs on the O atom of its NO^* moiety, forming (NOH^*–NO^* + CO^*) with a favorable Gibbs free energy (ΔG) change of –0.68 eV. In contrast, competitive reactions leading to HNO^*–NO^*/CO^*, NO^*–NO^*/COH^*, and NO^*–NO^*/CHO^* are endergonic, with ΔG values of 0.19~2.50 eV (Table S1). The approach of the second hydrogen results in the cleavage of the N–OH bond within (NOH^*–NO^* + CO^*) along the distal pathway, resulting in the formation of (N^*–NO^* + CO^*) and the release of one H_2O molecule. This process is downhill by 0.77 eV in the free energy profile. Subsequently, the (N^*–NO^* + CO^*) intermediate undergoes further hydrogenation to form (NH^*–NO^* + CO^*) with ΔG value of −1.06 eV. The fourth hydrogenation step, i.e., the hydrogenation of (NH^*–NO^* + CO^*), leads to the formation of the (NH_2^*–NO^* + CO^*) intermediate. Notably, this process is endergonic with a moderate Gibbs free energy uphill of 0.36 eV. Remarkably, the subsequent four PCET steps, transforming NH_2^*–NO^*/CO^* into (NH_2^*–NOH^* + CO^*), (NH_2^*–N^* + CO^*), (NH_2^*–NH^* + CO^*), and (NH_2^*–NH_2^* + CO^*) intermediates, are all exergonic, exhibiting ΔG values of −0.05, −1.14, −0.85, and −0.11 eV, respectively. What

follows is the non-PCET step: the separately adsorbed CO^* is inserted into the $NH_2^*–NH_2^*$ intermediate, coupling its two NH_2 moieties to form the $NH_2CONH_2^*$ product, which is considerably exergonic with a ΔG of −1.07 eV. Finally, the formed urea product is released from the Cu_4/Mo_2C surface, requiring only a small energy input of 0.19 eV.

Overall, in the one-step N–C–N coupling mechanism, the whole reaction process can be summarized as follows: $2NO + CO + {}^* \rightarrow NO^* + NO^* + CO^* \rightarrow NO^*–NO^* + CO^* \rightarrow NOH^*–NO^* + CO^* \rightarrow NO^*–N^* + CO^* \rightarrow NH^*–NO^* + CO^* \rightarrow NH_2^*–NO^* + CO^* \rightarrow NH_2^*–NOH^* + CO^* \rightarrow NH_2^*–N^* + CO^* \rightarrow NH_2^*–NH^* + CO^* \rightarrow NH_2^*–NH_2^* + CO^* \rightarrow NH_2^*–CO–NH_2^* \rightarrow$ urea + * (for details about the Gibbs free energy change for each step, see Supporting Information). These results identified the formation of ($NH_2^*–NO^* + CO^*$) as the potential-determining step (PDS) due to its maximum free energy increase of 0.36 eV. Thus, the limiting potential for the whole catalytic process is –0.36 V, which drives all elementary reaction steps exergonic. Notably, this limiting potential is less negative than those reported for several existing catalysts, such as V_N-Cu_3N-300 (−1.56 V),[29] Cu-Cu_2O (–0.58 V),[30] Cu(111),[31] atomic-scale copper,[32] suggesting the high activity of the Cu_4/Mo_2C catalyst.

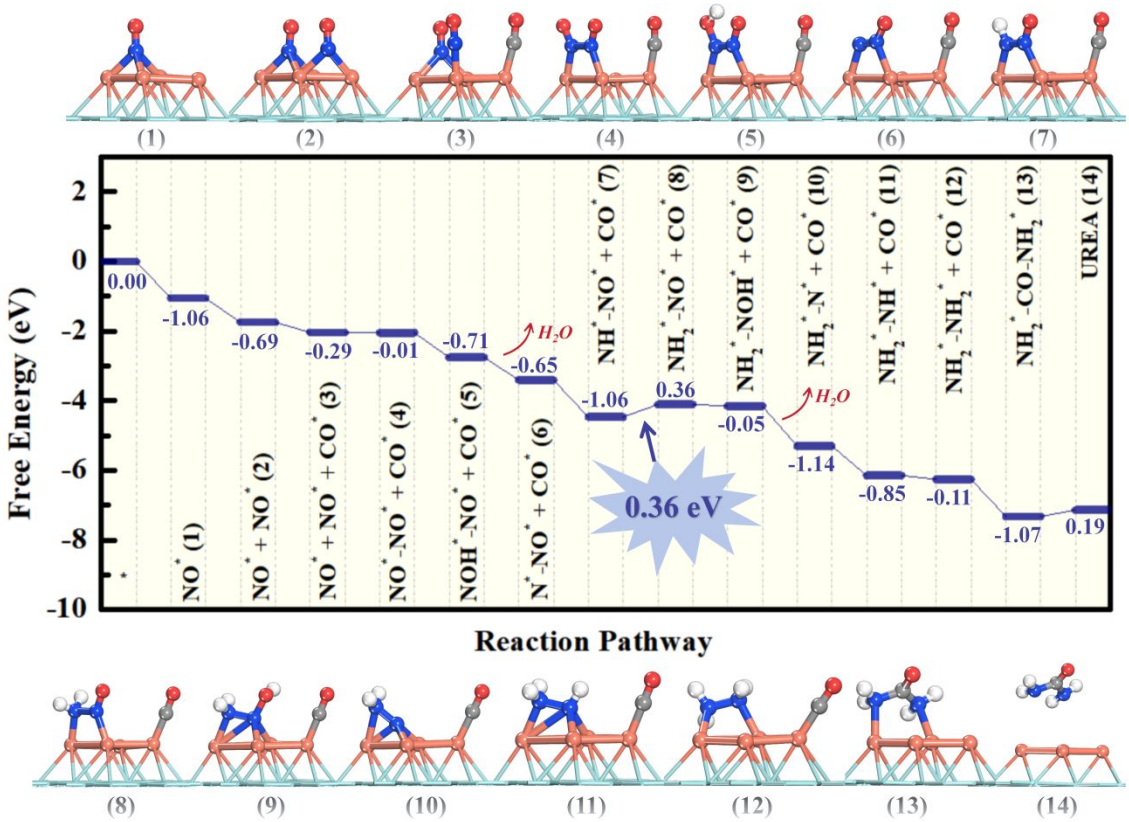

Fig. 3. Free energy diagram and optimized geometrical structures of the involved reaction intermediates for urea synthesis on Cu_4/Mo_2C through the one-step N–C–N coupling mechanism.

3.2.2. Two-step mechanism

We also investigated the possibility of producing urea through a two-step process based on previous studies:[14] initially NO* and CO* couple to form the *NO–CO* intermediate; subsequently, a further NO species addition yields NOCONO*, a critical precursor in urea synthesis.

Following the proposed mechanism, initially NO is chemisorbed on the Cu_4/Mo_2C substrate with the ΔG value of –1.06 eV, followed by the first C–N coupling with the co-adsorbed CO *via* the Eley–Raideal (ER) mechanism. The coupling process, (NO* + CO*) →

NO–CO, is exothermic (ΔG= –0.03 eV). The subsequent C–N coupling between *NO–CO* and NO* to form NOCONO* is uphill in the Gibbs free energy profile (ΔG= +0.10 eV). Upon formation of the NOCONO* intermediate, its hydrogenation to urea was investigated. Our computational analysis revealed that the energetically most preferred pathway from NOCONO* to urea on Cu_4/Mo_2C, as depicted in Fig. 4. These results showed that while most PCETs are exergonic, the steps to NH_2CONHO^* and $NH_2CONH_2^*$ are not spontaneous, with ΔG values of +0.16 eV and +0.45 eV, respectively.

From the calculated ΔG values, we identified the formation of $NH_2CONH_2^*$ intermediate as the PDS, due to its highest ΔG value of 0.45 eV among the elementary steps. Consequently, a limiting potential of –0.45 V is necessary for urea synthesis along the two-step mechanism, slightly more negative than that required for the one-step pathway (–0.36 V). Thus, the one-step N–C–N coupling mechanism is slightly more favorable energetically than the two-step mechanism.

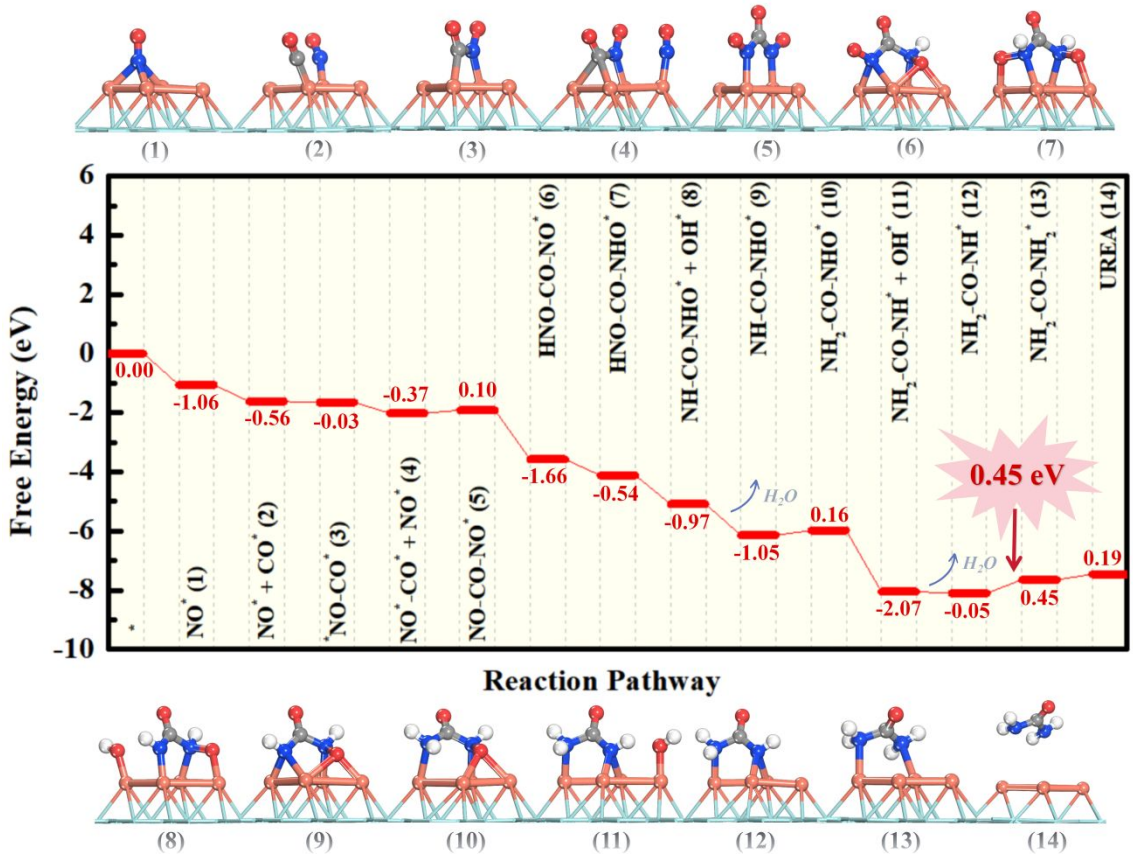

Fig. 4. Free energy diagram and optimized geometrical structures of the involved reaction intermediates for urea synthesis on Cu_4/Mo_2C through the two-step coupling mechanism.

3.2.3. Non-electrochemical C–N coupling

Besides the PCET steps, the non-electrochemical C–N coupling is the most challenging process during the process of urea formation. To gain a deeper understanding, we assessed the kinetic energy barriers for C–N coupling, examining both one–step and two–step mechanisms. Specifically, we analyzed two important C–N couplings occurring outside the PCET steps: $NH_2^*–NH_2^* + CO^* \rightarrow NH_2^*–CO–NH_2^*$ in the one–step mechanism, and $NO^* + CO^* \rightarrow {}^*NO–CO^*$, followed by ${}^*NO–CO^* + NO^* \rightarrow NO–CO–NO^*$ in the two–step mechanism. First, we computed the kinetic barrier for the one-step N–C–N coupling, where the CO^* is inserted into ${}^*NH_2–NH_2^*$, and found that this reaction step, $NH_2^*–NH_2^* + CO^* \rightarrow NH_2^*–CO–NH_2^*$,

requires a low energy barrier of 0.48 eV. This coupling process, with a free energy change (ΔG) of −1.07 eV, is considerably exergonic, indicating that it is favorable both thermodynamically and kinetically. Notably, the NH_2^* intermediate has been widely observed experimentally for urea synthesis from the co-reduction of CO_2 and NO_3^-, further confirming the feasibility of the one−step N–C–N coupling mechanism.[19-24]

To highlight the high feasibility of the one-step N–C–N coupling between $^*NH_2–NH_2^*$ and CO^*, we compared this reaction's efficiency with CO^*'s coupling with other nitrogenous species, including $^*NO–NO^*$, $^*NOH–NO^*$, $^*N–NO^*$, $^*NH–NO^*$, $^*NH_2–NO^*$, $^*NH_2–NOH^*$, $^*NH_2–N^*$, and $^*NH_2–NH^*$. Our analyses revealed that the couplings of CO^* with $^*NO–NO^*$, $^*NOH–NO^*$, and $^*N–NO^*$ are endergonic by 0.64, 0.52, and 0.27 eV (Fig. 5a), respectively, indicating their unfavorable thermodynamics. For the other five N–C–N coupling reactions, the kinetic barriers are in the range of from 0.64 to 3.77 eV (Fig. 5b), all higher than the barrier (0.48 eV) between $^*NH_2–NH_2^*$ and CO^* (0.48 eV). Thus, the $NH_2^*–NH_2^*$ + CO^* coupling is more advantageous, both thermodynamically and kinetically, compared to alternative N–C–N couplings.

A pertinent question emerges: why is $NH_2^*–NH_2^*$ the optimal precursor for the one-step N–C–N coupling? To address this question, using the Bader charge analysis, we examined the charges on various reaction intermediates, including CO^*, $^*NO–NO^*$, $^*NOH–NO^*$, $^*N–NO^*$, $^*NH–NO^*$, $^*NH_2–NO^*$, $^*NH_2–NOH^*$, $^*NH_2–N^*$, $^*NH_2–NH^*$, and $^*NH_2–NH_2^*$. As shown in Fig. 5c, the adsorbed CO^* species carries a negative charge throughout the reaction process. Among the N−containing intermediates, only $NH_2^*–NH_2^*$ is positively charged. This distinct charge disparity facilitates an electrostatic attraction between $NH_2^*–NH_2^*$ and CO^*, catalyzing the

N–C–N coupling through effective concurrent binding of CO^* to the two N atoms in NH_2^*–NH_2^*.

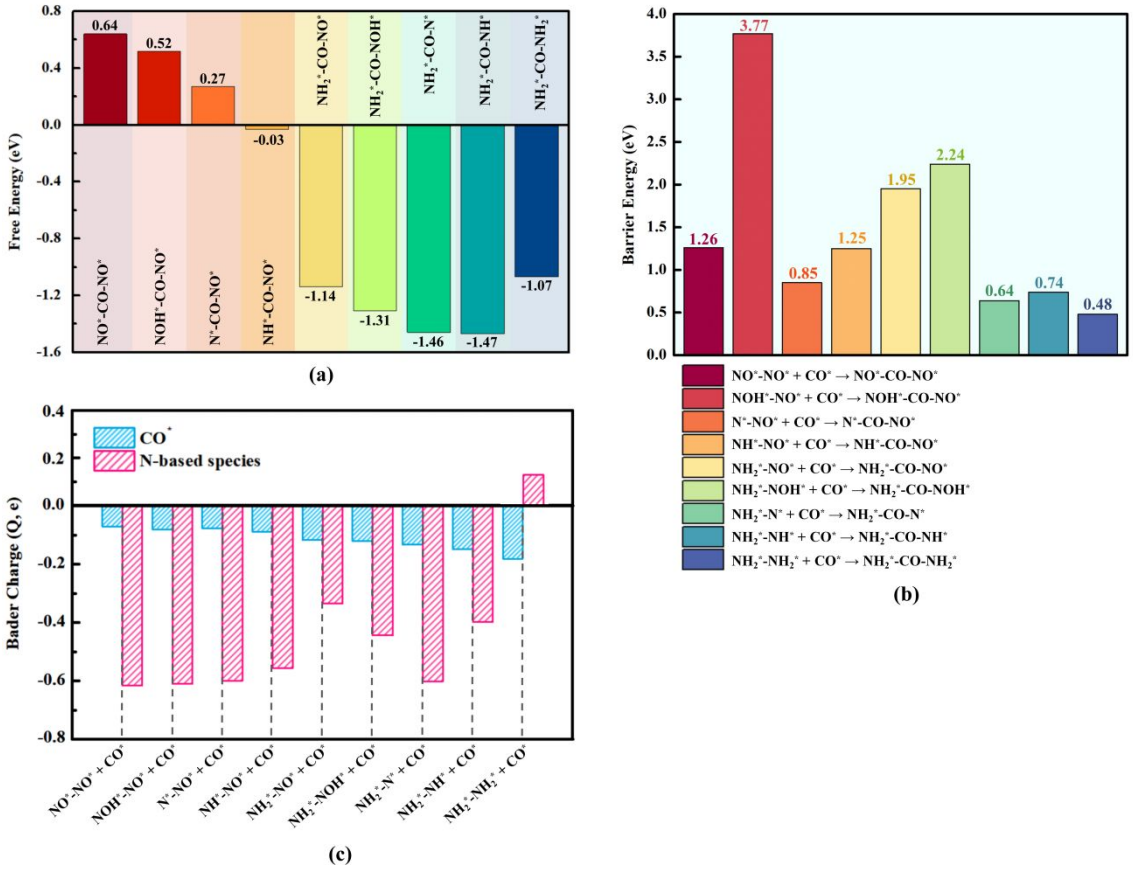

Fig. 5. (a) Free energy changes associated with the coupling of CO^* with various N-containing intermediates. (b) Minimum energy pathways for CO^* coupling with selected N–N dimers. (c) Computed charge on CO^* and different N-based species involved in the reaction.

On the other hand, in the two-step mechanism, we found that the energy barriers for the two sequential C–N coupling processes ($CO^* + NO^* \rightarrow {}^*CO–NO^*$, and ${}^*CO–NO^* + NO^* \rightarrow NOCONO^*$) are 0.58 and 1.47 eV (Fig. S3), respectively. The latter coupling emerges as the rate-determining step, with a barrier of 1.47 eV nearly threefold as compared with the one–step N–C–N mechanism's barrier (0.48 eV). Thus, we predicted that the urea synthesis on

Cu_4/Mo_2C is kinetically favored to proceed through the one–step N–C–N pathway, where CO^* is directly inserted into $^*NH_2–NH_2^*$.

3.2.4. Other Cu clusters supported on Mo_2C substrate

In addition to Cu_4/Mo_2C, we also examined the catalytic activity of other Cu clusters supported on Mo_2C substrate towards urea synthesis along the one-step pathway. Free energy diagrams for urea formation on these Cu clusters are presented in Fig. S4a. Interestingly, all these candidates share the same potential-determining step as Cu_4/Mo_2C, namely, $NH^*–NO^* + CO^* \rightarrow NH_2^*–NO^* + CO^*$, except for Cu_1/Mo_2C with the PDS of $NH^*–NO^* + CO^*$ formation. The ΔG values for the PDS vary from 0.40 to 0.53 eV, which are slightly higher than that on Cu_4/Mo_2C (0.36 eV, Fig. S4b), but lower than those reported for several recent catalysts (0.74~1.41 eV).[72-75] Consequently, these Cu clusters demonstrate substantial urea electrosynthesis activity.

To gain deep insights into the activity difference of these supported Cu clusters towards urea electrosynthesis, we explored the relationship between their activity and the adsorption strength of certain reaction intermediate, in line with the Sabatier principle. Notably, on Cu_1/Mo_2C surface, Cu and Mo sites are active sites (Fig. S5). Thus, we primarily examined the activity-adsorption strength relationship for intermediates on other Cu_n/Mo_2C (n = 2 ~ 7) systems, in which Cu atoms serve as the primary active sites. Excitingly, we observed a volcano plot between the urea production activity (U_L) and the adsorption energies of $NH_2^*–NO^*+ CO^*$ intermediate ($\Delta E_{NH2^*–NO^*+ CO^*}$), as depicted in Fig. 6a. The Cu_4/Mo_2C system stands at the apex of the volcano plot, consistent with its highest catalytic activity for

urea synthesis. Thus, the adsorption strength of NH_2^*–NO^*+ CO^* offers a reliable descriptor for understanding the catalytic trends across these Cu_n/Mo_2C materials.

To further explore the adsorption strength difference of NH_2^*–NO^*+ CO^*species on these catalysts, we calculated the d-band center (ε_d) of Cu-based active sites. The correlation between $\Delta E_{NH2^*–NO^*+\ CO^*}$ and ε_d, with the R^2 of 0.84 (Fig. 6b), suggests that the better catalytic activity of Cu_4/Mo_2C may originate from an optimal ε_d on the Cu active sites, which leads to its moderate binding with NH_2^*–NO^*+ CO^* intermediate. Thus, the SMSI between Cu_n clusters and Mo_2C substrate not only enhances the stability of the Cu_n clusters but also effectively optimizes their electronic properties for ideal interaction with reaction intermediates. This optimization is crucial for developing electrocatalysts that combine high durability with outstanding catalytic efficiency.

3.3. Catalytic Selectivity for Urea Formation

After confirming the highest activity of Cu_4/Mo_2C catalyst toward urea production, we assessed its selectivity for the one-step CO^* and NH_2^*–NH_2^* coupling to form NH_2^*–CO–NH_2^*, which could face competing reactions including CO^* desorption, CO^* hydrogenation, and NH_2^*–NH_2^* dissociation to NH_3. Our results showed that CO^* desorption and CO^* hydrogenation to COH^* and CHO^* are endergonic with ΔG values of 0.64, 1.60, and 0.97 eV, respectively (Fig. 6c). Furthermore, despite the further hydrogenation of NH_2^*–NH_2^* to NH_3 is exergonic (ΔG of −0.61 eV), it is less favorable than the C–N coupling (ΔG of −1.07 eV). This phenomenon is also evident in the anchored Cu_3, Cu_6, and Cu_7 clusters, whereas NH_3 production from NH_2^*–NH_2^*, with more negative ΔG values (Fig. S6), is more energetically

favorable on the Cu_1, Cu_2, and Cu_5 clusters. Consequently, the Cu_1, Cu_2, and Cu_5 clusters are excluded as suitable electrocatalysts for urea production since they prefer NH_3 synthesis.

Additionally, hydrogen evolution reaction (HER) is a potential competitive pathway in aqueous solution. Therefore, we examined the selectivity of Cu_n/Mo_2C toward HER and urea electrosynthesis by computing the free energy change of H^* adsorption (ΔG_{H^*}). Our results revealed that the H^* adsorption on the anchored Cu_4 cluster is relatively low, with ΔG_{H^*} values ranging from −0.30 to −0.48 eV (Fig. 6d and Fig. S6). This weak adsorption is primarily attributed to the electrostatic repulsion between the positively charged Cu atoms and H^+ ions. Especially, these ΔG_{H^*} values are less negative than both $\Delta G_{NO^*+NO^*}$ and $\Delta G_{NO^*+NO^*+CO^*}$ (Fig. 6e and Fig. S6), suggesting that urea formation is the predominant reaction on these Cu_n/Mo_2C catalysts.

Overall, the competing CO^* reduction/desorption, NH_3 formation, and HER can be greatly inhibited on some Cu_n/Mo_2C catalysts, including Cu_3, Cu_4, Cu_6, and Cu_7, ensuring the high selectivity of our as-designed Cu_n/Mo_2C catalysts toward urea formation. Thus, precisely controlling cluster size is advantageous for designing highly active and selective electrocatalysts.

3.4. Stability of the Catalyst under Realistic Aqueous Conditions

Beyond activity and selectivity, the durability of catalysts under realistic aqueous conditions is crucial for their practical applications in electrochemical reactions. Thus, we evaluated the stability of the Cu_n/Mo_2C systems by calculating their dissolution potential (U_{diss}, ESI), which serves as a measure of the dissolution resistance of Cu_n clusters from the substrate

into water. As expected, due to the rather strong interaction between the Cu_n clusters and the Mo_2C support, the computed U_{diss} values for these anchored Cu_n clusters are rather positive (0.49–0.64 V, Fig. S7), evidencing their outstanding stability under electrochemical conditions.

To examine whether the anchored Cu_n cluster might be covered by OH^*/O^* species in an aqueous solution during operation, we constructed the surface Pourbaix diagram to analyze their electrochemical stability across a wide range of pH values (0-14) and electrode potential (-1.5 to 3.0 V *vs*. SHE), where the Cu_4/Mo_2C system was selected a representative for its superior catalytic performance in urea electrosynthesis. We found that in strongly alkaline conditions and without applied potentials, the $Cu_4@Mo_2C$ surface is covered by OH^* species (Fig. 6f). However, applying a potential displaces these OH^* species, thereby exposing the active sites again. Notably, the minimum potential required to remove the surface OH^* species at pH = 14 is only −0.32 V, which is more positive than the limiting potential for urea production (−0.36 V). These findings suggest that Cu_4/Mo_2C exhibits good stability against surface oxidation under working conditions. To further substantiate the robust stability of Cu_4/Mo_2C, we conducted *ab initio* molecular dynamics (AIMD) simulations at 300 K over 10 ps with a 2 fs timestep. The simulations showed no significant structural distortion or bond dissociation, attesting to the high thermal stability of the Cu_4/Mo_2C system (Fig. S8).

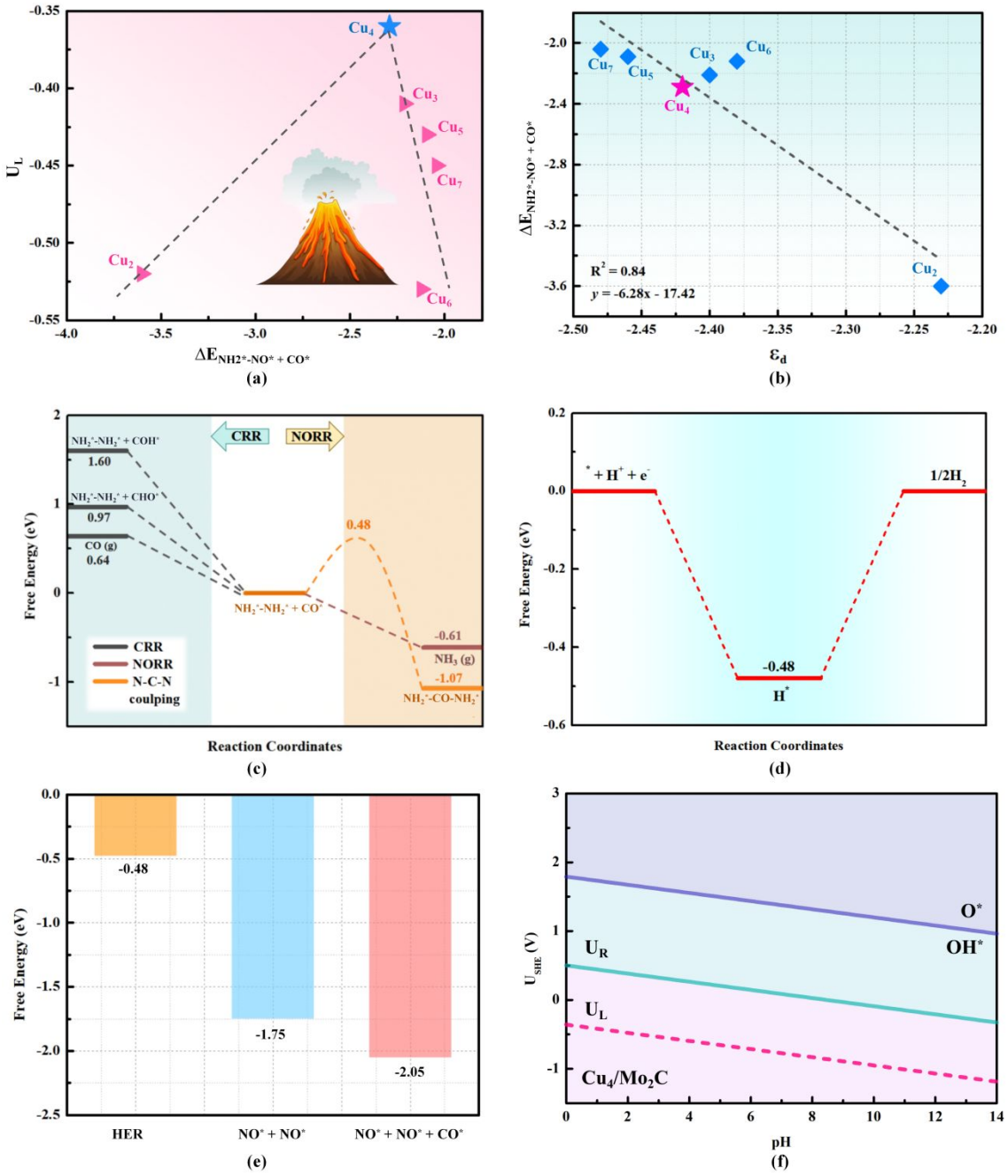

Fig. 6. (a) Volcano plot of adsorption energy of NH_2^*-NO^* + CO^* as a function of limiting potential of urea synthesis on Cu_n/Mo_2C (n = 2 ~ 7) systems. (b) The relationships of adsorption energy of NH_2^*–NO^* + CO^* with the variation of ε_d. (c) Reaction energy landscape for the subsequent reactions of co-adsorbed $^*NH_2$–$^*NH_2$ and CO^*. CRR refers to CO desorption, CO^* hydrogenation to COH^* and CHO^*. NORR refers to hydrogenation of NH_2^*–NH_2^* to NH_3. (d) Free energy profile for HER. (e) Comparison of hydrogen adsorption free energy (ΔG_{H^*})

with the adsorption free energies of (NO^* + NO^*) and (NO^* + NO^* + CO^*) on Cu_4/Mo_2C. (f) Surface Pourbaix diagrams of Cu_4/Mo_2C. Pink dashed line represents the limiting potential for urea formation (U_L). The blue-green line represents the redox potential (U_R).

Note that there have been no prior reports on the experimental synthesis of Cu clusters on 2D Mo_2C MXene, despite their superior catalytic performance for urea generation. To facilitate the practical application of these Cu_n/Mo_2C catalysts, we recommend several synthesis approaches. To synthesize 2D Mo_2C MXene, several studies can be used, including the carburization of molybdenum oxides at high temperatures,[76] etching layered ternary Mo_2Ga_2C with concentrated hydrofluoric acid,[77] molten copper-catalyzed chemical vapor deposition,[78] and a salt-assisted templating approach.[79] Furthermore, dispersed Cu clusters can be anchored on Mo_2C MXene through the wet impregnation deposition method with $CuCl_2.2H_2O$ aqueous solution as the metal precursor. Adjusting the concentration of precursors, solvent type, or adding additives (e.g., ligands) allows effective control over the growth rate and ultimate size of Cu clusters. Notably, similar approaches have successfully deposited Pt and Au nanoparticles of varied sizes onto Mo_2C MXene.[80-82] Therefore, we are confident that the synthesis of Cu_n/Mo_2C is rather feasible.

4. Conclusions.

In conclusion, based on the comprehensive DFT computations, we explored the potential of Cu clusters supported on Mo_2C monolayer as a promising catalyst for urea synthesis. The results showed that, due to the strong interaction, these Cu clusters favor to adhering to Mo_2C substrate in the planar pattern, which is beneficial to capture small molecules, such as NO and

CO. Moreover, by comparing the different reaction mechanisms, we found that the urea formation is preferable to proceed via a one-step concurrent N–C–N coupling mechanism both thermodynamically and kinetically, among which Cu_4 cluster exhibits the highest catalyst activity with a small limiting potential (–0.36 V) and a low energy barrier (0.48 eV). Especially, the competitive reactions, including CO reduction/desorption, NH_3 formation, HER, and O^*/OH^* coverage can be effectively suppressed, thus guaranteeing the high selectivity towards urea electrosynthesis. These findings offer a promising strategy to design and develop advanced catalysts for the synthesis of high-value-added organonitrogen chemicals from the catalytic coupling of carbonaceous and nitrogenous small molecules.

The authorship contribution statement

Yue Zhang: Conceptualization, Investigation, Formal analysis, Writing – original draft. **Linguo Lu:** Methodology, Validation, Investigation. **Tiantian Zhao:** Methodology, Synthesis of catalysts. **Jingxiang Zhao:** Conceptualization, Writing – review & editing, Supervision, Funding acquisition, Project administration, Resources. **Qinghai Cai:** Methodology. **Zhongfang Chen:** Project administration, Writing – review & editing.

NOTES

The authors declare no competing financial interest.

ACKNOWLEDGEMENT

This work was financially supported in China by the Natural Science Funds for Distinguished Young Scholar of Heilongjiang Province (No. JC2018004), and in the USA by

the Department of Energy, Office of Basic Energy Sciences under Award Number DE-SC0023418.

References

1. C. Chen, X. Zhu, X. Wen, Y. Zhou, L. Zhou, H. Li, L. Tao, Q. Li, S. Du, T. Liu, D. Yan, C. Xie, Y. Zou, Y. Wang, R. Chen, J. Huo, Y. Li, J. Cheng, H. Su, X. Zhao, W. Cheng, Q. Liu, H. Lin, J. Luo, J. Chen, M. Dong, K. Cheng, C. Li and S. Wang, *Nat. Chem.*, 2020, **12**, 717-724.

2. J. W. Erisman, M. A. Sutton, J. Galloway, Z. Klimont and W. Winiwarter, *Nat. Geosci.*, 2008, **1**, 636-639.

3. X. Zhu, X. Zhou, Y. Jing and Y. Li, *Nat. Commun.*, 2021, **12**, 080.

4. A. N. Rollinson, J. Jones, V. Dupont and M. V. Twigg, *Energy & Environ. Sci.*, 2011, **4**, 1216-1224.

5. M. Xia, C. Mao, A. Gu, A. A. Tountas, C. Qiu, T. E. Wood, Y. F. Li, U. Ulmer, Y. Xu, C. J. Viasus, J. Ye, C. Qian and G. Ozin, *Angew. Chem. Int. Ed.*, 2022, **61**, e202110158.

6. B. M. Comer, P. Fuentes, C. O. Dimkpa, Y.-H. Liu, C. A. Fernandez, P. Arora, M. Realff, U. Singh, M. C. Hatzell and A. J. Medford, *Joule*, 2019, **3**, 1578-1605.

7. J. Geng, S. Ji, M. Jin, C. Zhang, M. Xu, G. Wang, C. Liang and H. Zhang, *Angew. Chem. Int. Ed.*, 2023, **62**, e202210958.

8. F. Barzagli, F. Mani and M. Peruzzini, *Green Chem.*, 2011, **13**, 1267-1274.

9. S. Giddey, S. P. S. Badwal and A. Kulkarni, *Int. J. Hydrogen Energy*, 2013, **38**, 14576-14594.

10. N. Meng, X. Ma, C. Wang, Y. Wang, R. Yang, J. Shao, Y. Huang, Y. Xu, B. Zhang and Y. Yu, *ACS Nano*, 2022, **16**, 9095-9104.

11. M. Yuan, J. Chen, Y. Bai, Z. Liu, J. Zhang, T. Zhao, Q. Wang, S. Li, H. He and G. Zhang, *Angew. Chem. Int. Ed.*, 2021, **60**, 10910-10918.

12. X. Zhang, X. Zhu, S. Bo, C. Chen, K. Cheng, J. Zheng, S. Li, X. Tu, W. Chen, C. Xie, X. Wei, D. Wang, Y. Liu, P. Chen, S. P. Jiang, Y. Li, Q. Liu, C. Li and S. Wang, *Angew. Chem. Int. Ed.*, 2023, **62**, e202305447.

13. X. Peng, L. Zeng, D. Wang, Z. Liu, Y. Li, Z. Li, B. Yang, L. Lei, L. Dai and Y. Hou, *Chem. Soc. Rev.*, 2023, **52**, 2193-2237.

14. X. Wei, Y. Liu, X. Zhu, S. Bo, L. Xiao, C. Chen, T. T. T. Nga, Y. He, M. Qiu, C. Xie, D. Wang, Q. Liu, F. Dong, C.-L. Dong, X.-Z. Fu and S. Wang, *Adv. Mater.*, 2023, **35**, 2300020.

15. Y. Huang, R. Yang, C. Wang, N. Meng, Y. Shi, Y. Yu and B. Zhang, *ACS Energy Lett.*, 2022, **7**, 284-291.

16. C. Lv, L. Zhong, H. Liu, Z. Fang, C. Yan, M. Chen, Y. Kong, C. Lee, D. Liu, S. Li, J. Liu, L. Song, G. Chen, Q. Yan and G. Yu, *Nat. Sustain.*, 2021, **4**, 868-876.

17. Z. Tao, C. L. Rooney, Y. Liang and H. Wang, *J. Am. Chem. Soc.*, 2021, **143**, 19630-19642.

18. H. Wang, Y. Jiang, S. Li, F. Gou, X. Liu, Y. Jiang, W. Luo, W. Shen, R. He and M. Li, *Appl. Catal. B: Environ.*, 2022, **318**, 121819.

19. X. Liu, Y. Jiao, Y. Zheng, M. Jaroniec and S.-Z. Qiao, *Nat. Commun.*, 2022, **13**, 5471.

20. S. Liu, S. Yin, Z. Wang, Y. Xu, X. Li, L. Wang and H. Wang, *Cell Rep. Phys. Sci.*, 2022, **3**, 100869.

21. M. Jiang, M. Zhu, M. Wang, Y. He, X. Luo, C. Wu, L. Zhang and Z. Jin, *ACS Nano*, 2023, **17**, 3209-3224.

22. J. Li, Y. Zhang, K. Kuruvinashetti and N. Kornienko, *Nat. Rev. Chem.*, 2022, **6**, 303-319.

23. Y. Luo, K. Xie, P. Ou, C. Lavallais, T. Peng, Z. Chen, Z. Zhang, N. Wang, X.-Y. Li, I. Grigioni, B. Liu, D. Sinton, J. B. Dunn and E. H. Sargent, *Nat. Catal.*, 2023, **6**, (10), 939-948.

24. Y. Jiao, H. Li, Y. Jiao and S.-Z. Qiao, *J. Am. Chem. Soc.*, 2023, **145**, 15572-15580.

25. Y. Mao, Y. Jiang, Q. Gou, S. Lv, Z. Song, Y. Jiang, W. Wang, M. Li, L. Zheng, W. Su and R. He, *Appl. Catal. B: Environ.*, 2024, **340**, 123189.

26. N. Meng, Y. Huang, Y. Liu, Y. Yu, B. Zhang, *Cell Rep. Phys. Sci.*, 2021, **2**, 100378.

27. H. Wan, X. Wang, L. Tan, M. Filippi, P. Strasser, J. Rossmeisl and A. Bagger, *ACS Catal.*, 2023, **13**, 1926-1933.

28. L. Chen, C. Tang, Y. Zheng, K. Davey and Y. Jiao, *Sci. Chin. Mater.*, 2023, **66**, 2346-2353.

29. Z. Lv, S. Zhou, L. Zhao, Z. Liu, J. Liu, W. Xu, L. Wang and J. Lai, *Adv. Energy Mater.*, 2023, **13**, 2300946.

30. M. Qiu, X. Zhu, S. Bo, K. Cheng, N. He, K. Gu, D. Song, C. Chen, X. Wei, D. Wang, Y. Liu, S. Li, X. Tu, Y. Li, Q. Liu, C. Li and S. Wang, *CCS Chem.*, 2023, **5**, 2617-2627.

31. G.-L. Yang, C.-T. Hsieh, Y.-S. Ho, T.-C. Kuo, Y. Kwon, Q. Lu and M.-J. Cheng, *ACS Catal.*, 2022, **12**, 11494-11504.

32. S. Shin, S. Sultan, Z.-X. Chen, H. Lee, H. Choi, T.-U. Wi, C. Park, T. Kim, C. Lee, J. Jeong, H. Shin, T.-H. Kim, H. Ju, H. C. Yoon, H.-K. Song, H.-W. Lee, M.-J. Cheng and Y. Kwon, *Energy & Environ. Sci.*, 2023, **16**, 2003-2013.

33. Z. Luo, G. Zhao, H. Pan and W. Sun, *Adv. Energy Mater.*, 2022, **12**, 2201395.

34. T. W. van Deelen, C. Hernández Mejía and K. P. de Jong, *Nat. Catal.*, 2019, **2**, 955-970.

35. X. Sui, L. Zhang, J. Li, K. Doyle-Davis, R. Li, Z. Wang and X. Sun, *Adv. Energy Mater.*, 2022, **12**, 2102556.

36. J. Yang, W. Li, D. Wang and Y. Li, *Adv. Mater.*, 2020, **32**, 2003300.

37. T. Pu, W. Zhang and M. Zhu, *Angew. Chem. Int. Ed.*, 2023, **62**, e202212278.

38. G. Wang, R. Ma, N. Zhang, Y. Guo and K. Chu, *Chem. Commun.*, 2023, **59**, 13887-13890.

39. P. K. Roy and S. Kumar, *ACS Appl. Energy Mater.*, 2020, **3**, 7167-7179.

40. C. Wu, R. Li, Y. Wang, S. Lu, J. Lin, Y. Liua and X. Zhang, *Chem. Commun.*, 2020, **56**, 10046-10049.

41. R. Prachi and P. Devi, *Graphene and 2D mater.*, 2022, **7**, 107-117.

42. S. Yao, X. Zhang, W. Zhou, R. Gao, W. Xu, Y. Ye, L. Lin, X. Wen, P. Liu, B. Chen, E. Crumlin, J. Guo, Z. Zuo, W. Li, J. Xie, L. Lu, C. J. Kiely, L. Gu, C. Shi, J. A. Rodriguez and D. Ma, *Science*, 2017, **357**, 389-393.

43. S. K. Kim, Y.-J. Zhang, H. Bergstrom, R. Michalsky and A. Peterson, *ACS Catal.*, 2016, **6**, 2003-2013.

44. K. Chen, P. Shen, N. Zhang, D. Ma and K. Chu, *Inorg. Chem.*, 2023, **62**, 653-658.

45. X. Li, S. Wang, G. Wang, P. Shen, D. Ma and K. Chu, *Dalton Trans.*, 2022, **51**, 17547-17552.

46. G. Wang, R. Ma, N. Zhang, Y. Guo and K. Chu, *Chem. Commun.*, 2023, **59**, 13887-13890.

47. Z. Li, Y. Xiao, P. R. Chowdhury, Z. Wu, T. Ma, J. Z. Chen, G. Wan, T.-H. Kim, D. Jing, P. He, P. J. Potdar, L. Zhou, Z. Zeng, X. Ruan, J. T. Miller, J. P. Greeley, Y. Wu and A. Varma, *Nat. Catal.*, 2021, **4**, 882-891.

48. J. Zhao, L.-F. Yin, L.-X. Ling, R.-G. Zhang, M.-H. Fan and B.-J. Wang, *Catal. Sci. & Techn.*, 2022, **12**, 2542-2554.

49. G. Kresse and J. Hafner, *Phys. Rev. B*, 1993, **47**, 558-561.

50. G. Kresse and J. Furthmüller, *Phys. Rev. B*, 1996, **54**, 11169-11186.

51. P. E. Blochl, *Phys. Rev. B*, 1994, **50**, 17953-17979.

52. G. Kresse and D. Joubert, *Phys. Rev. B*, 1999, **59**, 1758-1775.

53. J. P. Perdew, K. Burke and M. Ernzerhof, *Phys. Rev. Lett.*, 1996, **77**, 3865-3868.

54. S. Grimme, *J. Comput. Chem.*, 2006, **27**, 1787-1799.

55. G. Henkelman, B. P. Uberuaga and H. Jónsson, *J. Chem. Phys.*, 2000, **113**, 9901-9904.

56. G. J. Martyna, M. L. Klein and M. Tuckerman, *J. Chem. Phys.*, 1992, **97**, 2635-2643.

57. J. K. Nørskov, J. Rossmeisl, A. Logadottir, L. Lindqvist, J. R. Kitchin, T. Bligaard and H. Jonsson, *J. Phys. Chem. B*, 2004, **108**, 17886-17892.

58. A. A. Peterson, F. Abild-Pedersen, F. Studt, J. Rossmeisl and J. K. Nørskov, *Energy & Environ. Sci.*, 2010, **3**, 1311-1315.

59. J. Wu, J. Su, T. Wu, Li. Huang, Q. Li, Y. Luo, H. Jin, J. Zhou, T. Zhai, D. Wang, Y. Gogotsi and Y. Li, *Adv. Mater.*, 2023, **35**, 2209954.

60. H. Zhou, Z. Chen, E. Kountoupi, A. Tsoukalou, P. M. Abdala, P. Florian, A. Fedorov and C. -R. Müller, *Nat. Commun.*, 2021, **12**, 5510.

61. Y. Yu, Z. Guo, Q. Peng, J. Zhou and Z. Sun, *J. Mater. Chem. A*, 2019, **7**, 12145-12153.

62. P. Calaminici, A. M. Köster, N. Russo and D. R. Salahub, *J. Chem. Phys.*, 1996, **105**, 9546-9556.

63. K. Jug, B. Zimmermann, P. Calaminici and A. -M. Köster, *J. Chem. Phys.*, 2002, **116**, 4497-4507.

64. A. -S. Chaves, G. -G. Rondina, M. -J. Piotrowski, P. Tereshchuk, and J. -L. F. D. Silva, *J. Phys. Chem. A*, 2014, **118**, 10813-10821.

65. X. Bai, Q. Li, L. Shi, X. Niu, C. Ling and J. Wang, *Small*, 2020, **16**, 1901981.

66. X. Liu, Y. Jiao, Y. Zheng, M. Jaroneic and S.-Z. Qiao, *Nat. Commun.*, 2022, **13**, 5471.

67. Q. Wu, C. Dai, F. Meng, Y. Jiao and Z. J. Xu, *Nat. Commun.*, 2024, **15**, 3335.

68. X. Fan, J. Cheng, M. Qiu, Y. Zhang, S. Chen, Z. Zhang, Y. Peng, J. Zhang and L. Zhang, *ACS Materials Lett.*, 2023, **5**, 1527–1531.

69. X. Liu, P. V. Kumar, Q. Chen, L. Zhao, F. Ye, X. Ma, D. Liu, X. Chen, L. Dai and C. Hu, *Appl. Catal. B: Environ.*, 2022, **316**, 121618.

70. X. Wei, X. Wen, Y. Liu, C. Chen, C. Xie, D. Wang, M. Qiu, N. He, P. Zhou, W. Chen, J. Cheng, H. Lin, J. Jia, X.-Z. Fu and S. Wang, *J. Am. Chem. Soc.*, 2022, **144**, 11530-11535.

71. N. Cao, Y. Quan, A. Guan, C. Yang, Y. Ji, L. Zhang and G. Zheng, *J. Colloid Interface Sci.*, 2020, **577**, 109-114.

72. J. Zhao, Y. Yuan, F. Zhao, W. Han, Q. Yuan, M. Kou, J. Zhao, C. Chen and S. Wang, *Appl. Catal. B: Environ.*, 2024, **340**, 123265.

73. X. Zhu, X. Yuan, Y. Wang, M. Ge and Y. Tang, *Journal of Catalysis*, 2024, **429**, 115218.

74. W. Zhang, M. Qu, A. Du and Q. Sun, *J. Mater. Sci.*, 2024, **59**, 5426-5435.

75. J. Liu, X. Lv, Y. Ma, S. -C. Smith, Y. Gu and L. Kou, *ACS Nano*, 2023, **17**, 25667-25678.

76. M. K. Kolel-Veetil, S. -B. Qadri, M. Osofsky, and Teddy M. Keller, *Chem. Mater.* 2005, **17**, 6101-6107.

77. J. Halim, S. Kota, M. -R. Lukatskaya, M. Naguib, M. Zhao, E. -J. Moon, J. Pitock, J. Nanda, S. J. May, Y. Gogotsi and M. -W. Barsoum, *Adv. Funct. Mater.*, 2016, **26**, 3118-3127.

78. D. Geng, X. Zhao, Z. Chen, W. Sun, W. Fu, J. Chen, W. Liu, W. Zhou and K. P. Loh, *Adv. Mater.*, 2017, **29**, 1700072.

79. J. Wu, J. Su, T. Wu, L. Huang, Q. Li, Y. Luo, H. Jin, J. Zhou, T. Zhai, D. Wang, Y. Gogotsi and Y. Li, *Adv. Mater.*, 2023, **35**, 2209954.

80. Y. -N. Regmi, G. -R. Waetzig, K. -D. Duffee, S. -M. Schmuecker, J. -M. Thodea and B. -M. Leonard, *J. Mater. Chem. A*, 2015, **3**, 10085-10091.

81. C. Wu, R. Li, Y. Wang, S. Lu, J. Lin, Y. Liua and X. Zhang, *Chem. Commun.*, 2020, **56**, 10046-10049.

82. P. Rajput and P. Devi, *Graphene and 2D mater.*, 2022, **7**, 107-117.